UDC 621.01:519.85:004.942 DOI 10.36910/775.24153966.2026.86.24

**Р. Р. Пишка**[0009-0005-0306-846X], **Б. Я. Бакай**[0000-0002-8707-9895]

*Національний лісотехнічний університет України*

## МЕТОД SIMP ІЗ ПРИСКОРЕННЯМ ЗБІЖНОСТІ ДЛЯ ТОПОЛОГІЧНОЇ ОПТИМІЗАЦІЇ НЕСУЧИХ ДЕТАЛЕЙ МАШИН

***Запропоновано модифікацію методу SIMP для топологічної оптимізації несучих елементів машинобудівних конструкцій – алгоритм FA-SIMP (Forward-Accelerated SIMP), який поєднує адаптивний крок випередження з керованим інерційним коефіцієнтом, побудованим за схемою FISTA, та подвійну проєкцію точки випередження на боксову й об'ємну допустимі множини. На відміну від класичної проєктовано-градієнтної схеми, у FA-SIMP чутливість обчислюється не в поточному наближенні, а у фізично допустимій точці випередження, зміщеній уздовж напрямку попереднього поступу, що змінює траєкторію оптимізації та прискорює спадання цільової функції. Для запобігання розбіжності в неопуклій задачі застосовано адаптивний рестарт імпульсу, який скидає інерцію в разі помітного зростання податливості. Такий підхід дає змогу оцінити не лише кінцеву жорсткість оптимізованої конструкції, а й стійкість самого ітераційного процесу за зміни геометрії та дискретизації. Метод досліджено на задачі мінімізації пружної податливості консольної балки у плоско-напруженому стані для трьох конфігурацій (A, B, C), що відрізняються геометричними розмірами та густиною скінченно-елементної сітки (від 2700 до 6480 елементів) за однакової об'ємної частки матеріалу, однакового бюджету ітерацій та конусної фільтрації поля чутливостей. Встановлено, що FA-SIMP стабільно знижує пружну податливість (до 3.95 %), індекс сірості (до 10.90 %) та максимальні переміщення (до 3.92 %), одночасно підвищуючи статичну жорсткість конструкції за незмінної маси й практично незмінного часу обчислень (у межах кількох відсотків). Ефект прискорення закономірно зростає з розмірністю задачі, а чіткіша бінаризація поля густин спрощує перенесення результату у CAD-модель. Отримані результати підтверджують, що крок випередження з подвійною проєкцією є практичним, сітково-стабільним прискоренням методу SIMP, придатним для автоматизованого проєктування полегшених несучих деталей машин.***

***Ключові слова:*** *топологічна оптимізація, SIMP, FA-SIMP, прискорений градієнтний спуск, крок випередження, консольна балка, скінченно-елементний аналіз, індекс сірості, сіткова стабільність.*

**R. R. Pyshka, B. Ya. Bakay**

## FORWARD-ACCELERATED SIMP FOR TOPOLOGY OPTIMIZATION OF LOAD-BEARING MACHINE PARTS

***A modification of the SIMP method for topology optimization of load-bearing elements of mechanical engineering structures is proposed – the FA-SIMP (Forward-Accelerated SIMP) algorithm, which combines an adaptive lookahead step governed by a FISTA-type momentum coefficient with a double box/volume projection of the lookahead point. The sensitivity is evaluated at a physically admissible lookahead point shifted along the previous descent direction, and an adaptive momentum restart reduces the risk of divergence in the non-convex problem. This approach makes it possible to assess not only the final stiffness of the optimized structure but also the stability of the iterative process under changes in geometry and discretization. The method is studied on compliance minimization of a cantilever beam for three configurations differing in physical size and finite-element mesh density. At the same volume fraction and iteration budget, FA-SIMP consistently reduces compliance (up to 3.95 %), grayness index (up to 10.90 %) and maximum displacement while preserving the prescribed mass and keeping the computation time practically unchanged, providing a mesh-stable acceleration of SIMP.***

***Keywords:*** *topology optimization, SIMP, FA-SIMP, accelerated gradient descent, lookahead step, cantilever beam, finite element analysis, grayness index, mesh stability.*

**Problem statement.** Rising requirements for energy efficiency, environmental performance and reliability of products stimulate the search for more refined methods of designing machine parts and assemblies [4]. In mechanical engineering this is especially relevant for load-bearing elements that operate under variable force, inertial and contact loads: brackets, base plates, levers, frame members, housing parts, mounting lugs and other critical components. During operation such parts carry loads from working bodies, drives, support nodes, and from the machine–environment interaction and the material is loaded non-uniformly – some regions carry the main share of the force flow, while others remain underloaded. It is precisely this non-uniformity that gives rise to stress-concentration zones near supports, attachment points, holes and points of application of external forces.

Traditional design of machine parts largely relies on inflated safety factors for strength and stiffness. As a consequence, the structure acquires excess mass, which degrades the energy efficiency of the machine, its dynamic behavior, material consumption and manufacturability. Therefore, one of the priority directions of modern mechanical engineering is the reduction of part mass while preserving the required strength, stiffness and operational reliability. The tools that allow this task to be addressed systematically at the design stage are the means of engineering analysis and shape optimization of critical parts [3].

Topology optimization stands out among such tools in that it automatically redistributes material within a prescribed design domain and produces a rational part shape in which the material is concentrated mainly along the principal force flows. This approach not only reduces mass but also raises the efficiency of material use, leaving material exactly in the zones that most affect the strength and stiffness of the product.

Among the density-based methods of topology optimization, SIMP (Solid Isotropic Material with Penalization) remains one of the most widely used. Despite its recognized advantages, classical SIMP has a number of limitations that complicate its application to real engineering problems [6]. The convergence of the basic scheme slows down at intermediate density values, especially for elongated or complexly loaded parts with a large ratio of characteristic dimensions. At the same time, mesh refinement degrades the binarization quality of the result: gray zones with intermediate density values accumulate in the design domain, which complicates the transfer of the solution to a CAD model. Finally, when the geometric proportions, boundary conditions and mesh density are changed, SIMP results may differ noticeably in compliance, grayness index and the character of the final topology, which raises the question of the mesh and geometric stability of the method.

Therefore, the practical use of topology optimization requires algorithms that combine efficient material redistribution with predictable convergence and reduced sensitivity to mesh parameters. Overcoming these limitations requires modifications of SIMP that simultaneously accelerate convergence, improve the discreteness of the density distribution and preserve the stability of the result when the geometric and mesh parameters change.

**Analysis of recent research and publications.** Topology optimization emerged as an independent research field after the seminal work of Bendsøe and Kikuchi [5], in which the optimal material-distribution problem was formulated on the basis of the homogenization approach. The further development of density methods is associated with the penalized interpolation of material properties, which laid the foundation of the SIMP method. Its canonical realization as the 99-line MATLAB code by Sigmund [6] established SIMP as a reference algorithm, while the generalized theoretical foundations of density methods, systematized in a monograph [7], shaped the subsequent development of the field.

A key role in ensuring the stability of numerical solutions is played by the regularization of the sensitivity field. Bourdin [8] showed that a cone filter of radius $r_{\min}$ effectively removes the characteristic "checkerboard" oscillations caused by low-order finite elements. Sigmund and Petersson [9] systematized the three main classes of numerical instabilities – the checkerboard effect, mesh dependence and local minima – and proposed a methodology for eliminating them by filtering and perimeter constraints. The improved implementation as an 88-line code with vectorized assembly of the stiffness matrix [10] became the base platform for subsequent modifications.

Subsequent studies focused on the suppression of gray elements. Lazarov and Sigmund [11] replaced the classical cone filter with a PDE filter based on the Helmholtz equation, ensuring independence of the result from the mesh structure, while Wang, Lazarov and Sigmund [12] combined such a filter with a Heaviside projection, which made it possible to control the sharpness of the material–void interface. Lian et al. [13] applied a hierarchical double penalization of intermediate densities, achieving a noticeable reduction of the grayness index without loss of stiffness. In the direction of mathematical analysis, Papadopoulos [14] proved the convergence of discrete SIMP solutions to continuous ones under mesh refinement provided correct regularization, while Sigmund and Maute [15] generalized the development of density, level-set and phase-field methods in a single review. Among the engineering generalizations, multiscale formulations [16] and multi-material extensions [17] are worth noting, which extend the basic SIMP to structures with functional gradients and combinations of different alloys.

A separate direction is associated with the acceleration of the iterative process. The idea of inertial acceleration of first-order methods goes back to the work of Beck and Teboulle [18], in which, for convex non-

smooth problems, an acceleration of convergence from $O(1/k)$ to $O(1/k^2)$ was proved by means of a lookahead step (FISTA). Although the SIMP problem is non-convex, in a number of numerical experiments inertial modifications of the OC scheme empirically demonstrate accelerated reduction of compliance without

additional global assumptions, which motivates the development of accelerated variants of the method.

Applied studies confirm the expediency of applying numerical modeling and optimization to load-bearing machine elements. Thus, in [1], modelling and dynamic analysis of an integrated system of lifting equipment were carried out, while in the work of Husachuk et al. [3], the QForm software was used to optimize the hot-die-forging process of a hydraulic-cylinder lug forging – a typical machine element. The application of topology optimization directly to load-bearing machine elements was considered by the authors in [2]. However, the available literature does not report a systematic comparison of classical SIMP with inertially accelerated variants on a series of similar cantilever problems differing in geometry and finite-element mesh parameters. This is precisely what determines the relevance of the present study.

**Research objectives.** The aim of the work is to increase the efficiency of the SIMP method for topology optimization of load-bearing elements of mechanical engineering structures by introducing an adaptive lookahead step, as well as a systematic assessment of the advantages of the resulting FA-SIMP algorithm over classical SIMP on a series of cantilever beams with different geometric dimensions and different finite-element mesh discretizations.

To achieve this aim, the following tasks were solved: the optimization problem of minimizing the elastic compliance of a cantilever beam under a volume constraint and box constraints on the densities was formalized; the classical SIMP algorithm with cone filtering and a projected-gradient update was described as the reference method; the FA-SIMP (Forward-Accelerated SIMP) algorithm with a FISTA-type adaptive inertial sequence and a double projection of the lookahead point was formulated; both methods were implemented in a common software environment and a comparative computation was performed on three cantilever configurations (A, B and C) with different physical dimensions and different numbers of finite elements; and the results were analyzed in terms of stiffness, topology quality and computational efficiency.

The expected practical result is the formulation of recommendations for applying FA-SIMP in the automated design of load-bearing machine parts with reduced material consumption, provided that the method remains stable when the relative dimensions of the cantilever and the finite-element mesh density are varied.

**Presentation of the main material.** We consider the problem of minimizing the elastic compliance of an isotropic two-dimensional plane-stress structure at a prescribed volume fraction of material:

$$\min_{\rho\in\mathrm{R}} C(\rho) = F^T U(\rho) \tag{1}$$

subject to

$$K(\rho)U(\rho) = F \tag{2}$$

$$\sum_{e=1}^{N} \rho_e V_e \leq V^* = f \sum_{e=1}^{N} V_e \tag{3}$$

$$\rho_{\min} \leq \rho_e \leq 1, e = 1,2,\dots,N \tag{4}$$

where $C(\rho)$ is the elastic compliance of the structure; $F$ is the vector of external nodal forces; $U(\rho)$ is the vector of nodal displacements; $K(\rho)$ is the global stiffness matrix of the system; $\rho = \{\rho_1, \dots, \rho_N\}$ is the vector of design variables (relative densities of $N$ finite elements); $V_e$ is the volume of the $e$-th element; $V^*$ is the admissible total volume; $f \in (0,1)$ is the prescribed volume fraction of material; $\rho_{\min} = 10^{-3}$ is the lower density bound that prevents degeneration of the stiffness matrix.

Equation (2) is the equilibrium condition of the finite-element model, inequality (3) bounds the total material volume, and relations (4) impose box constraints on each design variable. The work considers the classical compliance formulation without a stress constraint, which allows the effect of the algorithmic acceleration itself to be isolated.

The dependence of the element Young's modulus on its density is given by the SIMP power-law interpolation

$$E_e(\rho_e) = E_{\min} + \rho_e^p (E_0 - E_{\min}) \tag{5}$$

where $E_e(\rho_e)$ is the effective Young's modulus of the $e$-th element; $E_0$ = 210 GPa is the Young's modulus of the solid material (structural steel); $p = 3$ is the penalization exponent that makes intermediate densities energetically unfavorable and drives them towards the values 0 or 1; $E_{\min} = 10^{-9} E_0$ is the residual stiffness of void elements.

The minimum modulus is set as a very small fraction of the solid-material modulus and is used to ensure the numerical stability of the analysis in the presence of elements with zero or near-zero density. The discreteness of the density distribution is quantified by the grayness index

$$M_{\mathrm{nd}} = \frac{4\sum_e \rho_e(1-\rho_e)V_e}{\sum_e V_e}, \tag{6}$$

where the summation is taken over all elements, and $V_e$ are their volumes.

A value $M_{\mathrm{nd}} = 0$ corresponds to a perfectly binary distribution ($\rho_e \in \{0,1\}$), whereas $M_{\mathrm{nd}} = 1$ corresponds to a fully uniform field $\rho_e = 0.5$. Smaller values of $M_{\mathrm{nd}}$ mean sharper topology boundaries and a simpler transfer of the result to CAD documentation.

It is convenient to characterize the integral stiffness of the part by the static stiffness

$$k_{\mathrm{stat}} = \frac{F}{u_{\max}}, \tag{7}$$

where $F$ is the magnitude of the applied load, and $u_{\max}$ is the magnitude of the maximum nodal displacement.

A larger value of $k_{\text{stat}}$ corresponds to a stiffer structure under the same load.

The design domain is a two-dimensional rectangular plate in a plane-stress state of thickness $h$ = 12 mm, made of structural steel with Young's modulus $E_0$ = 210 GPa, Poisson's ratio $\nu$ = 0.30 and density $\rho_{\text{mat}}$ = 7870 kg/m³. All nodes of the left edge are rigidly clamped (all degrees of freedom fixed), and a concentrated vertical force $F$ = 8000 N directed downwards is applied at the midpoint of the right edge. This scheme reproduces the characteristic operation of a cantilever bracket or a base plate. In the immediate vicinity of the point of load application and of the left edge, small passive zones with $\rho \equiv 1$ are prescribed to avoid singular stress concentrations.

The basic SIMP algorithm is implemented in the form of a projected-gradient descent with cone filtering of the sensitivity field. At each $k$-th iteration the global stiffness matrix $K(\rho^{(k)})$ is assembled and the linear system (2) is solved by sparse LU factorization, after which the element-wise compliance sensitivity is computed

$$\frac{\partial C}{\partial \rho_e} = -p\rho_e^{p-1}(E_0 - E_{\min})u_e^T k_0 u_e, \tag{8}$$

where $u_e$ is the vector of nodal displacements of the $e$-th element; $k_0$ is the stiffness matrix of an element with unit Young's modulus; the remaining notation corresponds to equation (5).

The negative sign shows that increasing the element density reduces the compliance. The resulting sensitivity field is smoothed by a cone filter of radius $r_{\min}$, whose weight coefficient decays linearly with the distance between element centers

$$H_{ej} = \max\big(0, r_{\min} - \|x_e - x_j\|\big), \tag{9}$$

$$\frac{\partial \tilde{C}}{\partial \rho_e} = \frac{1}{\rho_e \sum_j H_{ej}} \sum_j H_{ej}\rho_j \frac{\partial C}{\partial \rho_j}, \tag{10}$$

where $H_{ej}$ is the weight coefficient of the influence of element $j$ on element $e$; $x_e$ and $x_j$ are the coordinates of their centers; and $\partial \tilde{C}/\,\partial \rho_e$ is the smoothed sensitivity.

Equation (10) reproduces the mesh-independence sensitivity filter of the Sigmund 99-line code [6]: the raw sensitivities are replaced by a weighted average normalized by the element density and by the sum of the weights, so that the filtered field remains consistent in magnitude. Filtering suppresses the checkerboard oscillations of the low-order four-node elements and enforces a minimum characteristic size of the load-bearing members of the topology.

The design variables are updated by a projected-gradient descent step with projection onto the admissible set

$$\rho_e^{(k+1)} = \mathrm{Proj}_{\mathcal{B}\cap\mathcal{V}}\left(\rho_e^{(k)} - s_k \frac{\partial \tilde{C}/\partial \rho_e}{\|\nabla \tilde{C}\|_\infty}\right), \tag{11}$$

where $s_k$ is the step size; $\|\nabla \tilde{C}\|_\infty$ is the normalizing factor (the maximum absolute value of the smoothed sensitivity); $\mathcal{B} = \{\rho : \rho_{\min} \le \rho_e \le 1\}$ is the box set; and $\mathcal{V} = \{\rho : \sum_e \rho_e V_e = V^*\}$ is the volume set.

The step size $s_k$ sets the descent step length, that is, how far the design moves along the normalized sensitivity direction at iteration $k$. Because the sensitivity is divided by its infinity norm $\|\nabla \tilde{C}\|_\infty$, the search direction is dimensionless and bounded in magnitude, so $s_k$ directly limits the largest density change of any element before projection. In this work $s_k$ is held constant over the iterations and is taken slightly larger for FA-SIMP than for SIMP, since the inertial step damps the oscillations that a larger raw step could otherwise induce; the chosen values are $s_k = 0.14$ for SIMP and $s_k = 0.22$ for FA-SIMP. A constant step keeps the comparison transparent and reproducible, while the per-iteration move limit and the subsequent projection guarantee that the update stays within the admissible set.

The projection $\mathrm{Proj}_{\mathcal{B}\cap\mathcal{V}}$ is implemented as a bisection over the Lagrange multiplier of the volume constraint followed by clipping to the box interval. The iterations continue until the convergence criterion (18) is satisfied or the maximum number of iterations is reached.

The proposed FA-SIMP algorithm extends the described scheme with an inertial lookahead step computed from the two previous approximations. The momentum coefficient is formed recursively by a scheme analogous to FISTA

$$t_0 = 1, t_{k+1} = \frac{1}{2}\left(1 + \sqrt{1 + 4t_k^2}\right), \tag{12}$$

$$\beta_k = \min\left(\frac{t_k - 1}{t_{k+1}}, \beta_{\max}\right), \tag{13}$$

where $t_k$ is an auxiliary cumulative parameter; $\beta_k$ is the momentum coefficient; and $\beta_{\max} = 0.62$ is its upper bound, which limits possible oscillations in the non-convex problem.

The sequence $\beta_k$ grows monotonically from zero (at $t_0 = 1$) to $\beta_{\max}$ over about four iterations, gradually strengthening the inertial step. Inside the parentheses of (13) the comma separates the two arguments of the min operator: the coefficient $\beta_k$ is taken as the smaller of the FISTA ratio $(t_k - 1)/t_{k+1}$ and the prescribed cap $\beta_{\max}$, so that the momentum can never exceed $\beta_{\max}$ even when the ratio approaches one.

The lookahead point is formed by adding the inertial shift

$$y^{(k)} = \rho^{(k)} + \beta_k\left(\rho^{(k)} - \rho^{(k-1)}\right), \tag{14}$$

where $y^{(k)}$ is the lookahead point, and $\rho^{(k)}$ and $\rho^{(k-1)}$ are the current and previous approximations.

To keep the point physically meaningful, it is necessarily projected onto the admissible set

$$y^{(k)} \leftarrow \mathrm{Proj}_{\mathcal{B}\cap\mathcal{V}}\left(y^{(k)}\right). \tag{15}$$

At the projected point $y^{(k)}$ the stiffness matrix, displacements and smoothed sensitivity are recomputed, after which a projected-gradient update step is performed

$$\rho_e^{(k+1)} = \mathrm{Proj}_{\mathcal{B}\cap\mathcal{V}}\left(y_e^{(k)} - s_k \frac{\widetilde{\partial C/\partial y_e}}{\|\nabla \widetilde{C}(y^{(k)})\|_\infty}\right), \tag{16}$$

that is, the update is applied to the values at the lookahead point, and the result is again projected onto $\mathcal{B} \cap \mathcal{V}$. The double projection is the defining difference of FA-SIMP from a plain addition of momentum to the step: it ensures that both the lookahead point $y^{(k)}$ and the new approximation $\rho^{(k+1)}$ simultaneously satisfy the box and volume constraints.

Since the problem is non-convex, the inertial step may cause the objective function to grow. To prevent divergence, an adaptive momentum restart is applied: if the compliance grows relative to the previous iteration by more than $\alpha_r = 6\%$, the cumulative parameter and the momentum coefficient are reset to their initial values

$$C^{(k+1)} > (1 + \alpha_r)C^{(k)} \Rightarrow t_{k+1} := 1, \beta_k := 0. \tag{17}$$

The iterative process stops by the density-stabilization criterion

$$\Delta_k = \max_e \left|\rho_e^{(k+1)} - \rho_e^{(k)}\right| < \varepsilon, \tag{18}$$

where $\Delta_k$ is the maximum element-wise density change between successive iterations, and $\varepsilon$ is a prescribed threshold; alternatively, the process stops when the maximum number of iterations $k_{\max} = 140$ is reached.

Both algorithms were implemented in Python 3.11 using sparse linear algebra (SciPy), vectorized operations (NumPy) and four-node isoparametric plane-stress elements; the computations were performed on an Apple M1 processor with 16 GB of RAM. The general parameters of the numerical experiment are listed in Table 1, and the geometric and mesh parameters of the three computational cases are listed in Table 2.

*Table 1*

**General parameters of the numerical experiment**

| Parameter | Value |
|---|---|
| Target volume fraction of material $f$ | 0.40 |
| SIMP penalization exponent $p$ | 3.0 |
| Cone filter radius $r_{\min}$, elem. | 2.4–2.6 |
| Upper bound of the momentum coefficient $\beta_{\max}$ | 0.62 |
| Adaptive restart threshold $\alpha_r$ | 0.06 |
| Density convergence criterion $\varepsilon$ | $5\cdot10^{-4}$ |
| Maximum number of iterations $k_{\max}$ | 140 |
| Young's modulus of the material $E_0$, GPa | 210 |
| Poisson's ratio $\nu$ | 0.30 |
| Material density $\rho_{\mathrm{mat}}$, kg/m³ | 7870 |
| Plate thickness $h$, mm | 12 |
| Concentrated load $F$, N | 8000 |

Case A corresponds to a compact bracket (aspect ratio 3:1, the coarsest mesh), case B to a cantilever of medium length (4.5:1, a moderately dense mesh), and case C to an elongated cantilever (5:1) with the largest number of finite elements. For all three cases the same initial density distribution $\rho_e^{(0)} = f = 0.40$ and the same maximum number of iterations were used, which ensures the correctness of the comparison of the methods.

*Table 2*

**Geometry and discretization of the computational cases**

| Case | Beam size $L_x \times L_y$, mm | Aspect ratio $L_x/L_y$ | Mesh $N_x \times N_y$ | Elements $N_{\text{el}}$ | Element size $\Delta x \times \Delta y$, mm | Filter radius $r_{\min}$, elem. |
|---|---|---|---|---|---|---|
| A | 300 × 100 | 3.00 | 90 × 30 | 2700 | 3.33 × 3.33 | 2.4 |
| B | 450 × 100 | 4.50 | 135 × 30 | 4050 | 3.33 × 3.33 | 2.4 |
| C | 600 × 120 | 5.00 | 180 × 36 | 6480 | 3.33 × 3.33 | 2.6 |

All six computations (three cases × two methods) converged by the prescribed criterion (18). A summary comparison of the engineering indicators is given in Table 3, and their percentage change on passing from SIMP to FA-SIMP in Table 4. This presentation makes it possible to compare both the absolute values of the engineering indicators and the relative gain obtained from the proposed acceleration in each computational case. Before turning to the analysis of the fields, we note a feature of the figure layout: the panels for cases A, B and C have different widths because the corresponding cantilevers differ in aspect ratio (3:1, 4.5:1 and 5:1) and are drawn at a single physical scale with the same scaling along the $x$ and $y$ axes; therefore, the longer cantilever naturally occupies a larger part of the figure. In all fields the top row ($a$) corresponds to classical SIMP, and the bottom row ($b$) to FA-SIMP.

*Table 3*

**Comparison of the engineering indicators of SIMP and FA-SIMP in the three cases**

| Case | Method | Compliance $C$, J | Grayness index $M_{\text{nd}}$ | Max. displacement $u_{\max}$, mm | Stiffness $k_{\text{stat}}$, N/mm | Mass $m$, kg | Time $t$, s |
|---|---|---|---|---|---|---|---|
| A | SIMP | 6.9658 | 0.3411 | 0.8751 | 9142 | 1.1351 | 9.81 |
| A | FA-SIMP | 6.9405 | 0.3369 | 0.8716 | 9179 | 1.1333 | 9.87 |
| B | SIMP | 20.7771 | 0.4034 | 2.6125 | 3062 | 1.7006 | 15.63 |
| B | FA-SIMP | 19.9564 | 0.3594 | 2.5100 | 3187 | 1.6999 | 16.04 |
| C | SIMP | 25.9305 | 0.3521 | 3.2569 | 2456 | 2.7219 | 30.12 |
| C | FA-SIMP | 25.1042 | 0.3220 | 3.1513 | 2539 | 2.7199 | 31.03 |

*Table 4*

**Percentage change of the metrics on passing SIMP → FA-SIMP**

| Case | $\Delta C$, % | $\Delta M_{\text{nd}}$, % | $\Delta u_{\max}$, % | $\Delta k_{\text{stat}}$, % | $\Delta m$, % | $\Delta t$, % |
|---|---|---|---|---|---|---|
| A | −0.36 | −1.23 | −0.40 | +0.40 | −0.16 | +0.55 |
| B | −3.95 | −10.90 | −3.92 | +4.09 | −0.04 | +2.57 |
| C | −3.19 | −8.53 | −3.24 | +3.35 | −0.08 | +3.01 |

A minus sign ("−") denotes a decrease of the corresponding quantity, and a plus sign ("+") its increase. For compliance, the grayness index, displacements and mass, a decrease is an improvement; for the static stiffness an improvement is an increase, whereas the increase of the computation time is a small price for the accelerated convergence.

As shown in Fig. 1, in all cases the topology takes the truss-like shape characteristic of a cantilever beam: diagonal struts are placed along the trajectories of the principal stresses and joined by horizontal chords. The advantages of FA-SIMP are most pronounced in case B, where the method forms noticeably sharper material–void interfaces, which corresponds to a reduction of the grayness index from 0.4034 to 0.3594 (by 10.90 %).

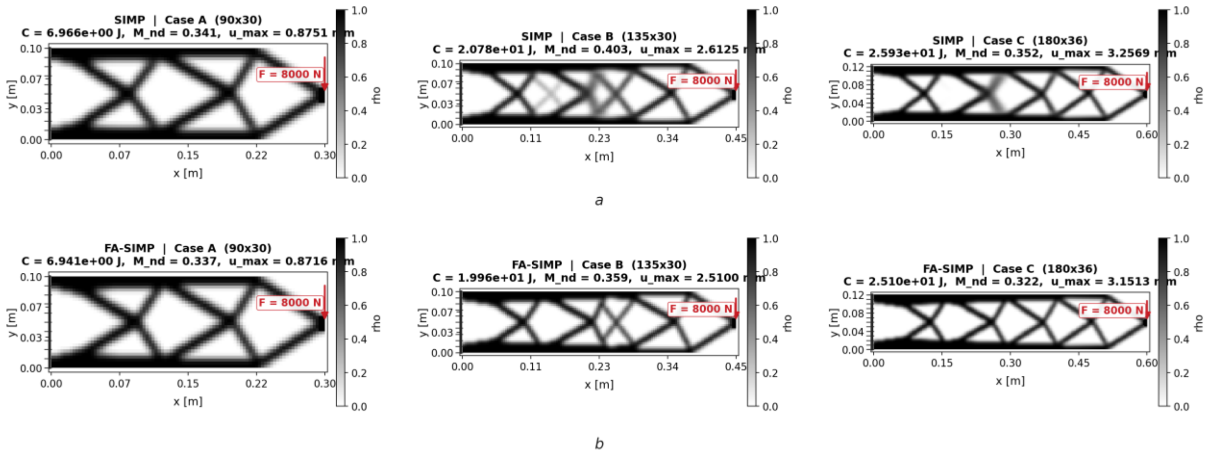


*Fig. 1.* **Final topologies for the three cases (columns A, B, C): *a* – SIMP (top row); *b* – FA-SIMP (bottom row). The scale $\boldsymbol{\rho_e \in [0, 1]}$ runs from white (void) to black (solid material)**

The distribution of the specific elastic strain-energy density $w_e = \frac{1}{2} u_e^T k(\rho_e) u_e$ (clipped at the 98.5th percentile) is shown in Fig. 2. In FA-SIMP the energy is distributed more uniformly along the working struts, without local overloads, which directly correlates with the lower compliance value. The corresponding displacement-magnitude field with an overlaid deformed mesh is shown in Fig. 3.

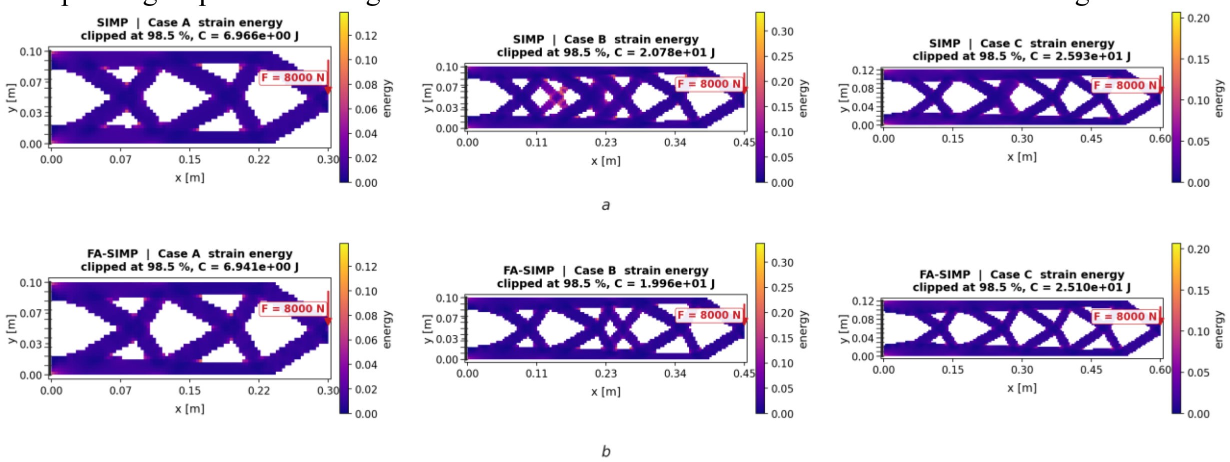


*Fig. 2.* **Specific elastic strain-energy density field (clipped at the 98.5th percentile) for the three cases: *a* – SIMP; *b* – FA-SIMP**

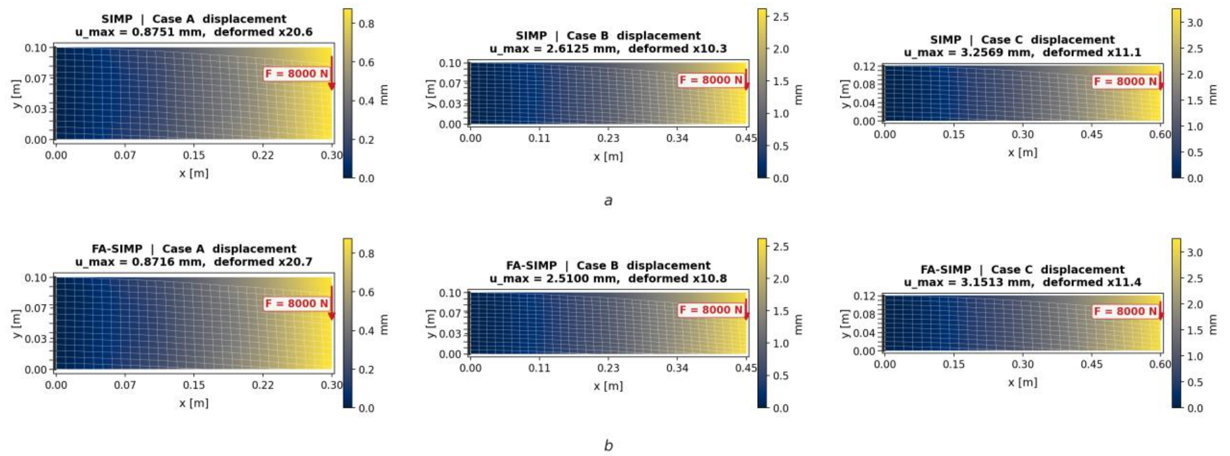


*Fig. 3.* **Nodal displacement-magnitude field (mm) with an overlaid deformed mesh: *a* – SIMP; *b* – FA-SIMP**

The convergence curves (Fig. 4) show that FA-SIMP steadily reaches a lower compliance value faster than classical SIMP. The steep drop of the compliance during the first $k \approx 20$–$30$ iterations is a consequence of the accumulated momentum $\beta_k \to \beta_{\max}$. The grayness-index dynamics of FA-SIMP shows a characteristic step – a fast drop to a quasi-asymptotic value, whereas SIMP approaches the same level noticeably more slowly.

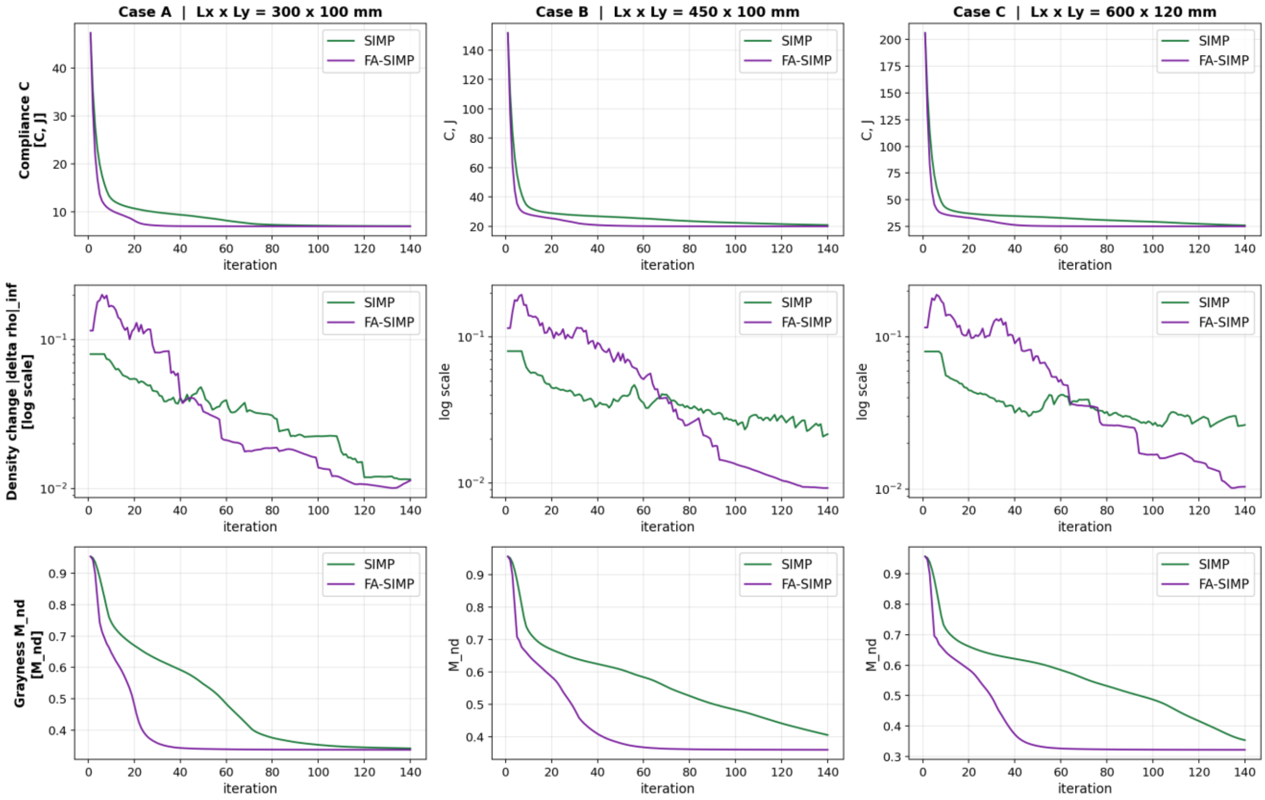


*Fig. 4.* **Convergence dynamics for the three cases: compliance $C$, maximum density change $\Delta_k$ and grayness index $M_{\mathrm{nd}}$**

A generalized comparison of all the key metrics is presented in Fig. 5. The structural mass in both methods is practically the same (difference less than 0.2 %), which confirms the exact fulfillment of the volume constraint, whereas the relative increase in computation time does not exceed 3.01 %. Thus, the additional computational cost of the proposed acceleration is negligible.

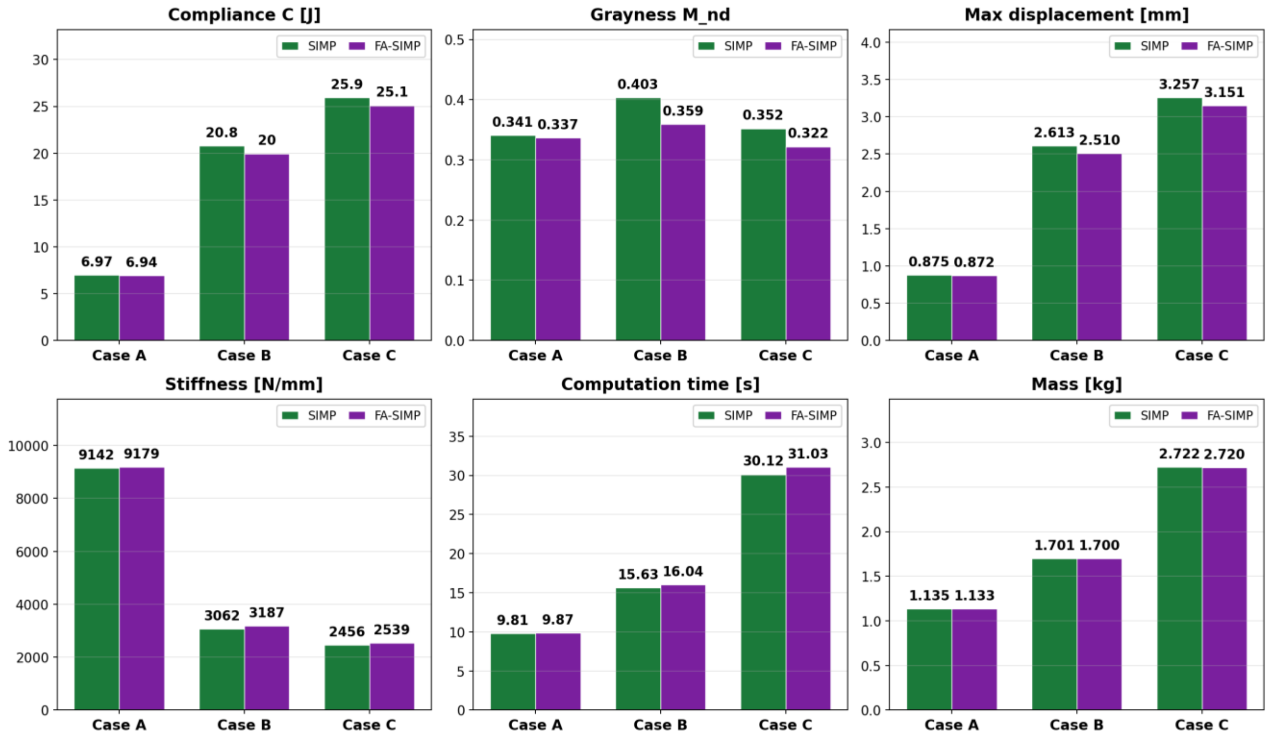


*Fig. 5.* **Summary comparison over six metrics: compliance, grayness index, maximum displacement, static stiffness, computation time and mass. SIMP – dark green, FA-SIMP – purple**

To complement the integral indicators, the local redistribution of material between the two optimized layouts was additionally analyzed. The density-difference field $\Delta\rho(x) = \rho^{\mathrm{FA}}(x) - \rho^{\mathrm{SIMP}}(x)$ (Fig. 6) visualizes the local differences between the two solutions: red zones correspond to the addition of material in FA-SIMP, blue zones to its removal. The averaged 1-norm of this field, computed by the formula

$$\|\Delta\rho\|_1 = \frac{1}{N}\sum_e \left|\rho_e^{\mathrm{FA}} - \rho_e^{\mathrm{SIMP}}\right|, \tag{19}$$

where $\rho_e^{\mathrm{FA}}$ and $\rho_e^{\mathrm{SIMP}}$ are the final element densities in the two methods, increases from case A to case C.

This reflects the strengthening of the acceleration effect as the problem dimensionality grows. The concentration of $\Delta\rho > 0$ at the truss-joint nodes and near the base of the cantilever shows that FA-SIMP consistently reinforces the regions that are critical for stiffness.

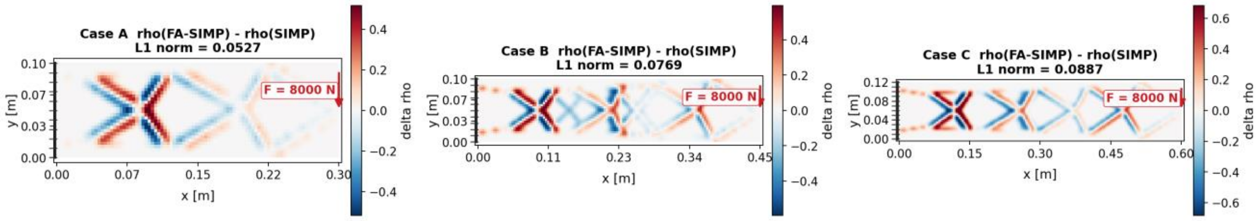


*Fig. 6.* **Final density-difference field $\boldsymbol{\Delta\rho = \rho^{\mathrm{FA}} - \rho^{\mathrm{SIMP}}}$ for the three cases: red zones – addition of material in FA-SIMP, blue – removal**

**Discussion of results.** A comparison of the three cases reveals several regularities in the behavior of FA-SIMP when the geometric and mesh parameters are changed. The most pronounced of them is the scaling of the acceleration effect with the problem size: in the smallest case A the compliance improvement is about 0.4 %, whereas in the larger cases B and C it reaches 3.19–3.95 %. This dependence is consistent with the motivation behind FISTA-type acceleration – in problems with a larger number of design variables and slower local convergence, the inertial step yields a larger gain.

The grayness index improves even more steadily than the compliance: in cases B and C the value $M_{\mathrm{nd}}$ decreases by 8.5–10.9 %, with the distribution becoming distinctly two-valued without the use of additional projection functions (in particular, the Heaviside projection). This means that the lookahead step plays the role of an implicit projection: oscillating elements with $\rho_e \approx 0.5$ receive an additional push towards the nearest binary value, which is consistent with the reduction of the grayness index reported in Table 4.

A natural consequence of the better convergence is the increase of the static stiffness for all three cases. Although the minimization of compliance and the maximization of stiffness are equivalent asymptotically, for a limited number of iterations these indicators may diverge. The fact that FA-SIMP simultaneously improves both the compliance and the displacements indicates the achievement of a better local optimum for the same computational budget, rather than a shift of the trade-off between stiffness and deformability.

At the same time, the computational cost of the acceleration remains disproportionately small. The additional operations of FA-SIMP are associated mainly with the formation and projection of the lookahead point, which are vector operations of order $O(N)$, whereas the dominant cost, as in classical SIMP, falls on the solution of the finite-element system. This is exactly why the computation times of the two methods differ insignificantly – within a few percent.

The obtained results should be considered with the limitations of the study in mind. All experiments were performed on two-dimensional plane-stress models, whereas real load-bearing machine parts have a three-dimensional geometry and require verification of the method on hexahedral and tetrahedral elements. A single load case was considered, although typical load-bearing elements experience a spectrum of loads. Three points in the parameter space $(L_x/L_y, N_{\mathrm{el}})$ were studied, whereas a strict limit passage under mesh refinement for a fixed geometry should be carried out separately. A sensitivity analysis with respect to the parameters $\beta_{\max}$, $r_{\min}$ and $p$, which were taken standard for all cases, was also not performed. At the same time, the generalization of FA-SIMP to three-dimensional problems does not require conceptual changes – only the computational kernel (three-dimensional element stiffness matrices) changes, which outlines a natural direction for further research.

**Conclusions.** The aim of the work was to increase the efficiency of the SIMP method for topology optimization of load-bearing elements of mechanical engineering structures. It was achieved by introducing an adaptive lookahead step with controlled momentum built according to the FISTA scheme, together with a double projection of the lookahead point onto the box and volume sets, which jointly form the FA-SIMP algorithm. The reference SIMP and the proposed FA-SIMP were implemented in a common environment and compared on identical cantilever benchmarks, so that the differences reported below are attributable to the acceleration mechanism alone.

The key mechanism behind the improvement is that the sensitivity in FA-SIMP is evaluated not at the current iterate but at a physically admissible lookahead point shifted forward along the direction of the previous progress. Because the design at which the gradient is sampled already anticipates the descent, the method follows a more efficient trajectory and reaches a better local optimum within the same iteration budget. This mechanism can explain the simultaneous improvement of several indicators – a faster drop of the compliance, a sharper binarization of the density field and a higher static stiffness – that in a fixed-budget run would otherwise trade off against one another. The double projection keeps both the lookahead point and the new iterate inside the box and volume sets, so the mass is held at the prescribed level: the part is lightened not by removing mass but by redistributing the same mass more rationally.

The numerical experiment quantified a clear tendency between the problem dimensionality and the gain from acceleration. As the number of design variables grows, the local convergence of classical SIMP slows down, and the inertial step compensates for this slowdown, so the effect of FA-SIMP grows accordingly – from a fraction of a percent in the smallest case (0.36 % in compliance) to 3.19–3.95 % in compliance and 8.5–10.9 % in the grayness index in the larger cases, while the maximum displacement decreases by up to 3.92 % and the static stiffness increases by up to 4.09 %. Since the additional operations are of order $O(N)$ and do not change the dominant cost of solving the finite-element system, the acceleration leaves the computation time practically unaffected – the difference between the methods stays within a few percent, and the structural mass differs by less than 0.2 %.

Two findings are of particular methodological value. First, the lookahead step acts as an implicit binarization: without any Heaviside or other projection function, FA-SIMP yields a markedly more discrete density field, which is precisely the property that classical SIMP lacks and that usually has to be enforced by extra penalization. Second, the gains were obtained with a single, unchanged set of algorithmic parameters across three different aspect ratios and mesh densities, which indicates the mesh and geometric stability of the method and distinguishes it from accelerations that require case-by-case retuning.

The practical value of the obtained results is that FA-SIMP produces a sharper and more stable material distribution when the geometry and mesh density are varied, and therefore reduces the amount of manual post-processing of the topology and simplifies the transfer of the result to a CAD model of load-bearing machine parts. Prospects for further research are associated with extending the method to three-dimensional problems, accounting for the spectrum of operational loads, and integrating it with the assessment of fatigue life.

**References:**


1. Loveikin V., Romasevych Y., Bakay B., Rudko I., Radiak I. Modelling and Dynamic Analysis of an Integrated Hydraulic Forest Crane-Winch System for Timber Extraction. FME Transactions. 2025. Vol. 53, No. 4. P. 625–638. DOI: https://doi.org/10.5937/fme2504625L.
2. Pyshka R., Bakay B. Improvement of the SIMP method for topology optimization of load-bearing elements of forest machinery structures. Forestry Education and Science: Current Challenges and Development Prospects (ICBSDW 2026). 2026. URL: https://conf.nltu.edu.ua/index.php/nltu150/article/view/511.
3. Husachuk D. A., Klymenko O. D., Parfentieva I. O., Dmytriiuk M. V., Imbirovych N. Yu., Feshchuk Yu. P., Karpiuk M. M. Optimization of the hot-die-forging process of a hydraulic-cylinder lug forging in the QForm software. Naukovi Notatky. 2021. Iss. 72. P. 80–87. DOI: https://doi.org/10.36910/775.24153966.2021.72.12.
4. Liu J., Ma Y. A survey of manufacturing oriented topology optimization methods. Advances in Engineering Software. 2016. Vol. 100. P. 161–175. DOI: https://doi.org/10.1016/j.advengsoft.2016.07.017.
5. Bendsøe M. P., Kikuchi N. Generating optimal topologies in structural design using a homogenization method. Computer Methods in Applied Mechanics and Engineering. 1988. Vol. 71, No. 2. P. 197–224. DOI: https://doi.org/10.1016/0045-7825(88)90086-2.
6. Sigmund O. A 99 line topology optimization code written in Matlab. Structural and Multidisciplinary Optimization. 2001. Vol. 21, No. 2. P. 120–127. DOI: https://doi.org/10.1007/s001580050176.

7. Bendsøe M. P., Sigmund O. Topology Optimization: Theory, Methods and Applications. 2nd ed. Berlin; Heidelberg: Springer, 2004. 370 p. DOI: https://doi.org/10.1007/978-3-662-05086-6.
8. Bourdin B. Filters in topology optimization. International Journal for Numerical Methods in Engineering. 2001. Vol. 50, No. 9. P. 2143–2158. DOI: https://doi.org/10.1002/nme.116.
9. Sigmund O., Petersson J. Numerical instabilities in topology optimization: A survey on procedures dealing with checkerboards, mesh-dependencies and local minima. Structural Optimization. 1998. Vol. 16. P. 68–75. DOI: https://doi.org/10.1007/BF01214002.
10. Andreassen E., Clausen A., Schevenels M., Lazarov B. S., Sigmund O. Efficient topology optimization in MATLAB using 88 lines of code. Structural and Multidisciplinary Optimization. 2011. Vol. 43, No. 1. P. 1–16. DOI: https://doi.org/10.1007/s00158-010-0594-7.
11. Lazarov B. S., Sigmund O. Filters in topology optimization based on Helmholtz-type differential equations. International Journal for Numerical Methods in Engineering. 2011. Vol. 86, No. 6. P. 765–781. DOI: https://doi.org/10.1002/nme.3072.
12. Wang F., Lazarov B. S., Sigmund O. On projection methods, convergence and robust formulations in topology optimization. Structural and Multidisciplinary Optimization. 2011. Vol. 43, No. 6. P. 767–784. DOI: https://doi.org/10.1007/s00158-010-0602-y.
13. Lian R., Jing S., He Z., Shi Z. A Hierarchical Double Penalty Method of Gray-Scale Elements for SIMP in Topology Optimization. Journal of Computer-Aided Design & Computer Graphics. 2020. Vol. 32, No. 8. P. 1349–1356. DOI: https://doi.org/10.3724/SP.J.1089.2020.18064.
14. Papadopoulos I. P. A. Numerical analysis of the SIMP model for the topology optimization problem of minimizing compliance in linear elasticity. Numerische Mathematik. 2025. Vol. 157, No. 1. P. 213–248. DOI: https://doi.org/10.1007/s00211-024-01438-3.
15. Sigmund O., Maute K. Topology optimization approaches: A comparative review. Structural and Multidisciplinary Optimization. 2013. Vol. 48, No. 6. P. 1031–1055. DOI: https://doi.org/10.1007/s00158-013-0978-6.
16. Gao J., Luo Z., Li H., Gao L. Topology optimization for multiscale design of porous composites with multi-domain microstructures. Computer Methods in Applied Mechanics and Engineering. 2019. Vol. 344. P. 451–476. DOI: https://doi.org/10.1016/j.cma.2018.10.017.
17. Li D., Kim I. Y. Multi-material topology optimization for practical lightweight design. Structural and Multidisciplinary Optimization. 2018. Vol. 58, No. 3. P. 1081–1094. DOI: https://doi.org/10.1007/s00158-018-1953-z.
18. Beck A., Teboulle M. A Fast Iterative Shrinkage-Thresholding Algorithm for Linear Inverse Problems. SIAM Journal on Imaging Sciences. 2009. Vol. 2, No. 1. P. 183–202. DOI: https://doi.org/10.1137/080716542.

**Reviewer: O. A. Kuzin,** Doctor of Technical Sciences, Associate Professor, Department of Applied Mechanics and Mechanical Engineering Technology, Ukrainian National Forestry University.

Дата надходження статті до видання: 27.03.2026
Дата прийняття статті до друку після рецензування: 24.05.2026
Дата оприлюднення 28.05.2026